

range  $2 \leq d_p \leq 3 \mu\text{m}$  are reliable for LDV measurements in these conditions.

The conditions at impact are given in Fig. 3. The ratio ( $\phi_i/\phi_{en}$ ) between the angle  $\phi$  that the particles impact the cylinder and the corresponding one they enter the boundary layer, is of the order of 1, increasing towards 1.5 for the larger particles. The angle of impact  $\beta$  (with respect to the local tangent on the cylinder) is nearly 90° for the smaller particles and drops almost linearly to 30° for the larger ones. The ratio of the particle momentums between impact and the initial point, is of the order of 5–15%, the particles nearer to the axis exhibiting a larger reduction. The particle temperature at impact for the smaller particles is close to  $T_w$  (indicative of a very fast cooling) but for the larger particles is somewhat in the middle between  $T_w$  and  $T_\infty$ .

### CONCLUSIONS

The deposition of sub-micrometre ash particles near the leading edge of cylindrical surfaces, under conditions representative of gas turbine blades and boiler superheater tubes has been investigated by calculating their trajectories and impact conditions.

The results indicate:

(i) The influence of the thermophoretic force is drastic. Use of sub-micrometre particles in LDV measurements in such flow fields should be avoided.

(ii) Such particles upon entering the boundary layer are attracted very quickly towards the surface. Their momentum, however, has been reduced significantly at impact, although their temperature is somewhere in the middle between the inviscid flow temperature and the wall temperature. Thus, although they impact in a normal direction, they do not have enough momentum to rebound.

(iii) The capture height of these particles is very small, when compared to the cylinder radius, being of the order of 0.001.

### REFERENCES

1. G. Vermes, Thermophoresis-enhanced deposition rates in combustion turbine blade passages, *Trans. ASME J. Engng Pwr* **101**, 542–548 (October 1979).
2. S. C. Saxena, R. F. Henry and W. F. Podolski, Particulate removal from high-temperature, high-pressure combustion gases, *Prog. Energy Combust. Sci.* **11**, 193–251 (1985).
3. J. A. Laitone, Characterization of particle rebound phenomena in the erosion of turbomachinery, *J. Aircraft* **20**(3), 275–281 (March 1983).
4. D. Kladas and D. P. Georgiou, Hot particles over cylinders in non-isothermal flow, *Proc. Tech. Chamber of Greece* (submitted) (in Greek).
5. G. K. Batchelor, *An Introduction to Fluid Dynamics*, Cambridge University Press, London (1970).
6. M. E. Crawford and W. M. Kays, STAN5—a program for numerical computation of two-dimensional internal and external boundary layer flows, NASA CR-2742 (1976).
7. E. W. Adams and J. P. Johnson, A mixing length model for the prediction of convex curvature effects on turbulent boundary layers, *Trans. ASME J. Engng Gas Turbine Pwr* **106**(1), 142–148 (January 1984).
8. F. M. White, *Viscous Fluid Flow*, p. 323, McGraw-Hill, New York (1974).
9. H. Schlichting, *Boundary Layer Theory* (6th Edn), p. 475, McGraw-Hill, New York (1968).
10. D. P. Georgiou, Hot particles in transpired non-isothermal laminar stagnation zones, *ASME, 1987, Cogenturbo Symp. Proc.*, pp. 349–354 (1987).
11. J. R. Brock, On the theory of thermal force on aerosol particles, *J. Colloid Interface Sci.* **17**, 768–774 (1962).
12. L. Talbot *et al.*, Thermophoresis of particles in a heated boundary layer, *J. Fluid Mech.* **101**(4), 737–758 (1980).
13. E. Auchenbach, Total and local heat transfer from a smooth cylinder in gross-flow of high Reynolds numbers, *Int. J. Heat Mass Transfer* **18**, 1387–1396 (1975).

## Laminar-flow heat transfer to a fluid flowing axially between cylinders with a uniform wall heat flux

O. MIYATAKE

Department of Chemical Engineering, Kyushu University, Fukuoka 812, Japan

and

H. IWASHITA

Toyokohan Co., Ltd., Kudamatsu 744, Japan

(Received 5 November 1989 and in final form 14 February 1990)

### 1. INTRODUCTION

IN REGARD to the laminar-flow heat transfer to a fluid flowing axially between cylinders, several analytical [1, 2] and numerical [3–5] asymptotic solutions applicable in the region of large axial distance are available for a triangular array [1–5] and a square array [5] of cylinders with a uniform wall temperature peripherally and a uniform wall heat flux axially [1, 2, 4], and with a uniform wall heat flux peripherally and axially [2–5]. However, little is known about the charac-

teristics of axially varying heat transfer in this geometry, although such characteristics are required for the design of multitubular heat exchangers for highly viscous liquid and rod-bank regenerators.

Thus, in the previous paper [6], the characteristics of axially varying heat transfer to a fluid flowing axially between a triangular array or a square array of cylinders with a uniform peripheral and axial wall temperature were analyzed using a finite-difference technique. Here, attention is directed to analyzing the case of cylinders with a uniform peripheral and axial wall heat flux.

**NOMENCLATURE**

*A* dimensionless flow area per cylinder (equation (11))  
*a, b* coefficient and exponent, respectively (equation (19))  
*c<sub>p</sub>* heat capacity of fluid at constant pressure [J kg<sup>-1</sup> K<sup>-1</sup>]  
*d<sub>o</sub>* diameter of cylinder [m]  
*f, g* functions of  $\sigma$  (equations (15) and (16), respectively)  
*Gz<sub>loc</sub>* local Graetz number,  $wc_p/(kz)$   
*h<sub>loc</sub>* local heat transfer coefficient,  $q_w/(\bar{t}_w - t_0)$  [W m<sup>-2</sup> K<sup>-1</sup>]  
*k* thermal conductivity of fluid [W m<sup>-1</sup> K<sup>-1</sup>]  
*Nu<sub>loc</sub>* local Nusselt number,  $h_{loc}d_o/k$   
*q<sub>w</sub>* wall heat flux [W m<sup>-2</sup>]  
*R* dimensionless radial coordinate,  $r/r_o$   
*r* radial coordinate [m]  
*r<sub>o</sub>* radius of cylinder [m]  
*s* half pitch between cylinders [m]  
*T* dimensionless temperature,  $(t - t_0)/(q_w r_o/k)$   
*t* temperature [K]  
*V* dimensionless axial velocity,  $v/v_m$   
*v* axial velocity of fluid [m s<sup>-1</sup>]  
*v<sub>m</sub>* mean axial velocity of fluid [m s<sup>-1</sup>]  
*w* mass flow rate of fluid per cylinder [kg s<sup>-1</sup>]  
*Z* dimensionless axial coordinate,  $z\alpha/(r_o^2 v_m)$   
*z* axial coordinate [m].

Greek symbols

$\alpha$  thermal diffusivity of fluid [m<sup>2</sup> s<sup>-1</sup>]  
 $\varepsilon$  volume fraction of cylinders (equation (13))  
 $\eta$  interior division ratio of local Nusselt number (equation (17))  
 $\theta$  angular coordinate [rad]  
 $\theta^+$  opening angle of analytical element (equation (6)) [rad]  
 $\rho$  density of fluid [kg m<sup>-3</sup>]  
 $\sigma$  pitch-to-diameter ratio,  $s/r_o$  ( $=2s/d_o$ )  
 $\phi$  dimensionless spacing between cylinders,  $\sigma - 1$ .

Superscript

$\bar{x}$  peripherally averaged,  $\int_0^{\theta^+} x d\theta/\theta^+$ .

Subscripts

b fluid bulk mean  
 w cylinder wall  
 0 inlet, asymptote for small  $z$   
 $\infty$  asymptote for large  $z$ .

Abbreviations

[SA] square array  
 [TA] triangular array.

**2. MATHEMATICAL FORMULATION AND METHOD OF NUMERICAL ANALYSIS**

The analytical system and coordinates are shown in Fig. 1. The following assumptions are made for the analysis of laminar-flow heat transfer to a fluid flowing axially between a triangular array or a square array of cylinders of diameter  $d_o$ , radius  $r_o$ , length  $z$ , and spaced  $2s$  apart: (1) there is a uniform peripheral and axial heat flux  $q_w$  on the wall of each cylinder in the heat transfer region ( $z \geq 0$ ); (2) the fluid enters the heat transfer region at a uniform temperature  $t_0$  and flows through the heat transfer region with a fully developed laminar-flow velocity distribution; and (3) axial heat conduction through the fluid is negligible in comparison with the convective transfer.

Under these assumptions, the dimensionless energy equation and the dimensionless thermal boundary conditions take the form:

$$V \frac{\partial T}{\partial Z} = \frac{1}{R} \frac{\partial}{\partial R} \left( R \frac{\partial T}{\partial R} \right) + \frac{1}{R^2} \frac{\partial^2 T}{\partial \theta^2} \quad (1)$$

$$Z = 0; \quad T = 0 \quad (2)$$

$$R = 1; \quad \partial T / \partial R = -1 \quad (3)$$

$$R = R^+; \quad (\partial T / \partial R) \cos \theta - (\partial T / \partial \theta) (\sin \theta / R) = 0 \quad (4)$$

$$\theta = 0, \theta = \theta^+; \quad \partial T / \partial \theta = 0 \quad (5)$$

where

$$\left. \begin{aligned} V &= \frac{v}{v_m}, \quad T = \frac{t - t_0}{q_w r_o / k}, \quad R = \frac{r}{r_o}, \quad Z = \frac{z\alpha}{r_o^2 v_m}, \quad \sigma = \frac{s}{r_o} \\ R^+ &= \sigma / \cos \theta, \quad \theta^+ = \pi/6 \text{ [TA]}, \quad \theta^+ = \pi/4 \text{ [SA]} \end{aligned} \right\} \quad (6)$$

[TA] or [SA] represents a triangular array or a square array of cylinders, respectively.

The dimensionless velocity  $V$  was evaluated from the analytical expression presented by Sparrow and Loeffler [7] by using recalculated and newly calculated coefficients in the expression as shown in ref. [6].

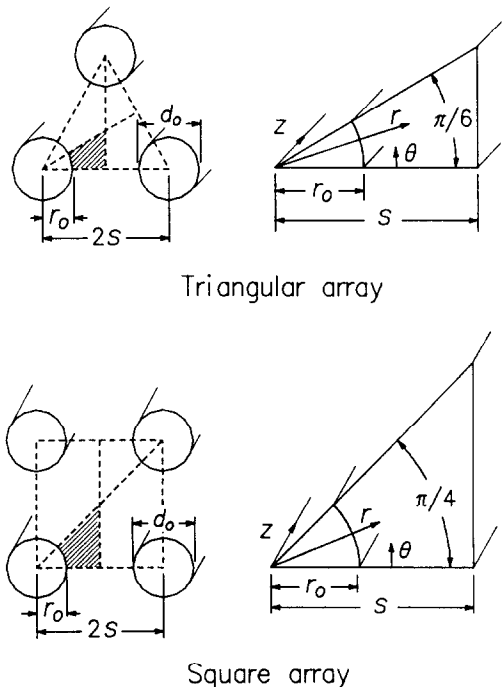


FIG. 1. Analytical system and coordinates.

The local Nusselt number  $Nu_{loc}$  is given by

$$Nu_{loc} = \frac{h_{loc} d_0}{k} = \frac{2}{\bar{T}_w - T_b} \quad (7)$$

where  $\bar{T}_w$  is the dimensionless peripherally averaged temperature on the wall of the cylinder and  $T_b$  the dimensionless bulk temperature given by

$$T_b = \frac{t_b - t_0}{q_w r_0 / k} = \int_0^{\theta^+} \int_1^{R^+} TVR \, dR \, d\theta / \int_0^{\theta^+} \int_1^{R^+} VR \, dR \, d\theta \quad (8)$$

The local Graetz number  $Gz_{loc}$  may be defined as

$$Gz_{loc} = w c_p / (kz) = A/Z \quad (9)$$

where  $w$  and  $A$  respectively represent the mass flow rate of fluid per cylinder and the dimensionless cross-sectional flow area per cylinder given by

$$w = v_m \rho r_0^2 A \quad (10)$$

$$A = 2\sqrt{3}\sigma^2 - \pi \text{ [TA]}, \quad A = 4\sigma^2 - \pi \text{ [SA]} \quad (11)$$

In the region of large local Graetz number ( $z \rightarrow 0$ ), the asymptotic solution of Bird [8], obtained by assuming that the velocity distribution in the thin thermal boundary layer is linear, can be extended to give the following expression for the asymptotic local Nusselt number:

$$Nu_{loc,0} = \frac{2\Gamma(2/3)}{(9A)^{1/3}} \left\{ \left( \frac{\partial V}{\partial R} \right)^{-1/3} \right\}^{-1} Gz_{loc}^{1/3} \quad (12)$$

The present analysis was performed by the forward-marching, implicit method with iteration, in which the convergent solution of the finite-difference form of the energy equation was obtained by the implicit method iteratively on each new level of  $Z$ . The detailed procedure is to be found in ref. [9].

The first step was to calculate  $V$  at each nodal point for a given value of  $\sigma$ , then to set the boundary condition for  $Z = 0$ , and to begin the calculation at a very low value of  $Z$  corresponding to a local Graetz number greater than  $5 \times 10^7$ .

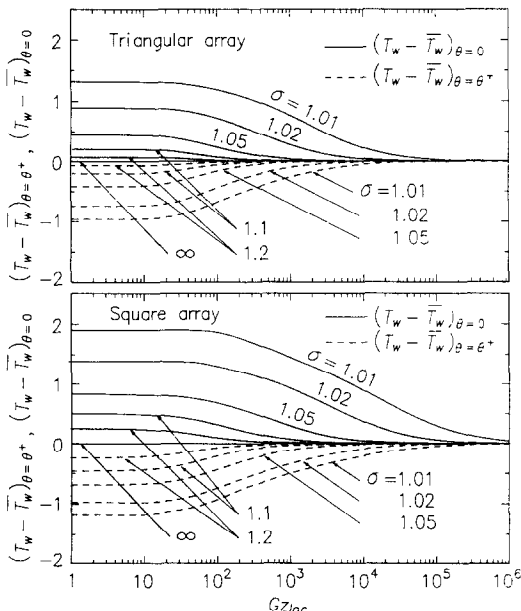


FIG. 2. Variation of wall temperature with local Graetz number.

The iterative calculation for each level of  $Z$  was terminated when the absolute values of the differences between the values of  $T$  at all the nodal points in the  $R$ - and  $\theta$ -directions before and after the iteration were below  $10^{-5}$ . The calculations then advanced to the next level of  $Z$ .

### 3. RESULTS OF NUMERICAL ANALYSIS

Figure 2 shows the relationship between the local wall-to-peripherally averaged wall temperature difference ( $T_w - \bar{T}_w$ ) at  $\theta = 0$  and  $\theta^+$  and the local Graetz number  $Gz_{loc}$ , with the pitch-to-diameter ratio  $\sigma$  as a parameter. It appears that peripheral variation of the wall temperature increases with the decrease of  $\sigma$  and  $Gz_{loc}$ , because the smaller the pitch and the larger the axial distance, the more a cylinder is influenced by the presence of the neighboring cylinders.

Figure 3 shows the relationship between the asymptotic local wall-to-peripherally averaged wall temperature difference ( $T_w - \bar{T}_w$ ), and the angular coordinate  $\theta$ , with  $\sigma$  as a parameter. The wall temperature  $T_w$  decreases in the circumferential direction from a maximum at  $\theta = 0$  (the hot spot) to a minimum at  $\theta = \theta^+$ . For  $\sigma > 1.1$  [TA] or 1.2 [SA],  $T_w$  is essentially uniform around the circumference.

Figure 4 shows the relationship between the local Nusselt number  $Nu_{loc}$  and the local Graetz number  $Gz_{loc}$ , with  $\sigma$  as a parameter. As seen from the figure, in the region of large  $Gz_{loc}$ ,  $Nu_{loc}$  increases as  $\sigma$  is reduced and tends to converge toward equation (12) represented by the broken lines. In the region of small  $Gz_{loc}$ ,  $Nu_{loc}$  increases and then decreases suddenly as  $\sigma$  is reduced. The reason for this behavior is that, as  $\sigma$  is reduced, the decrease in the flow area increases the velocity gradient at the wall (see Fig. 6) and thereby increases  $Nu_{loc}$ ; below a certain value of  $\sigma$ , however, the velocity of fluid in the location of narrow flow area decreases and the wall temperature increases at  $\theta \approx 0$  (see Fig. 3) and thereby decreases  $Nu_{loc}$ .

Figure 5 shows the comparison between numerical results for a uniform wall heat flux  $\textcircled{\text{H}}$  and those for a uniform wall

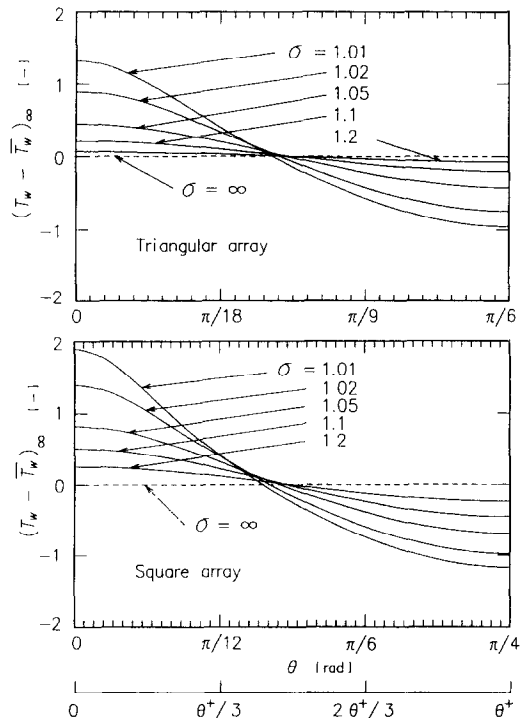


FIG. 3. Peripheral variation of asymptotic wall temperature.

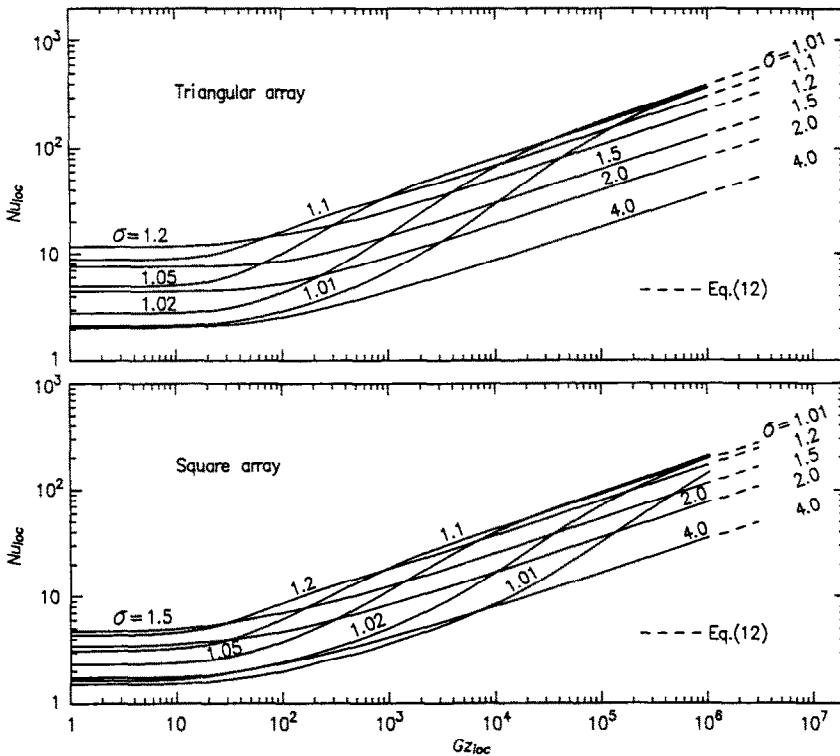


FIG. 4. Variation of local Nusselt number with local Graetz number.

temperature  $\textcircled{T}$  [6]. For relatively large  $\sigma$ , the difference between the values of  $Nu_{loc}$  in each case is small; as  $\sigma$  approaches unity, however, the decrease in  $Nu_{loc}$  in the region of small  $Gz_{loc}$  becomes larger for the case of  $\textcircled{H}$  due to the increase in the wall temperature at  $\theta \approx 0$ .

Figure 6 shows the relationship between the asymptotic local Nusselt number  $Nu_{loc,\infty}$  in the region of small local Graetz number and the dimensionless spacing between cylinders  $\phi (= \sigma - 1)$  together with the corresponding information obtained from the numerical results of Dwyer-Berry [4] and the graphical results of Antonopoulos [5] (see also Table 1). In each case,  $Nu_{loc,\infty}$  increases and then decreases as  $\sigma$  is reduced.  $\{(\partial V/\partial R)_w^{-1/3}\}^{-1}$  in equation (12) is also shown in Fig. 6.

Figure 7 shows the comparison between numerical results for a triangular array (the solid lines) and those for a square array (the broken lines) at the same values of volume fraction of cylinders  $\varepsilon$  given by

$$\varepsilon = \frac{\pi r_o^2}{2\sqrt{3}s^2} = \frac{\pi}{2\sqrt{3}\sigma^2} \text{ [TA]}, \quad \varepsilon = \frac{\pi r_o^2}{4s^2} = \frac{\pi}{4\sigma^2} \text{ [SA]}. \quad (13)$$

As seen from the figure, in general,  $Nu_{loc}$  for a triangular array is larger than that for a square array at the same values of  $\varepsilon$ , especially for the case of  $\varepsilon > 0.5$ . The difference between  $Nu_{loc}$  for each array of cylinders is reduced as  $\varepsilon$  is decreased.

#### 4. CORRELATING EQUATIONS FOR THE NUSSELT NUMBER

A formula suitable for prediction of the local Nusselt number can be derived by making use of the asymptotic local Nusselt numbers  $Nu_{loc,0}$  given by equation (12) and  $Nu_{loc,\infty}$  obtained by the present numerical analysis.

The numerical solutions for  $\{(\partial V/\partial R)_w^{-1/3}\}^{-1}$  and  $Nu_{loc,\infty}$  can be formulated in the following way (see broken lines in Fig. 6):

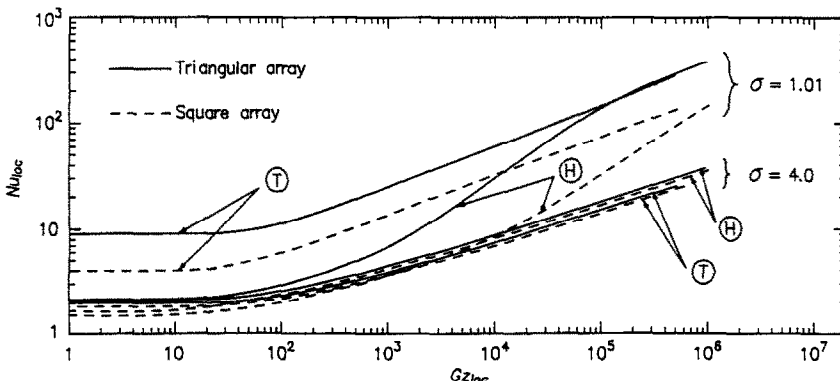


FIG. 5. Comparison of local Nusselt number for two thermal wall boundary conditions ( $\textcircled{H}$ , uniform wall heat flux;  $\textcircled{T}$ , uniform wall temperature [6]).

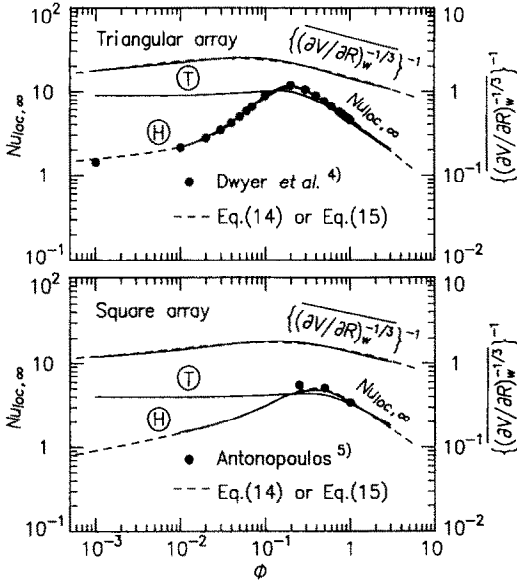


FIG. 6. Variation of asymptotic local Nusselt number and dimensionless quantity to velocity gradient at the wall with dimensionless spacing between cylinders (⊕, uniform wall heat flux; ⊙, uniform wall temperature [6]).

$$\left. \begin{aligned} \left\{ \left( \frac{\partial V}{\partial R} \right)_w^{-1/3} \right\}^{-1} &= \frac{1.180(1 + 8.24\phi^{0.39}) / (1 + 6.37\phi^{0.73})}{\left\{ \left( \frac{\partial V}{\partial R} \right)_w^{-1/3} \right\}^{-1}} \text{ [TA]} \\ &= \frac{0.940(1 + 4.40\phi^{0.39}) / (1 + 2.66\phi^{0.73})}{\left\{ \left( \frac{\partial V}{\partial R} \right)_w^{-1/3} \right\}^{-1}} \text{ [SA]} \end{aligned} \right\} \quad (14)$$

$$\left. \begin{aligned} Nu_{loc,\infty} &= (3.1\phi^{0.1} + 324\phi^{1.6}) / (1 + 69.5\phi^{2.4}) = f \text{ [TA]} \\ Nu_{loc,\infty} &= (3.6\phi^{0.2} + 32.2\phi^{1.5}) / (1 + 9.1\phi^{2.2}) = f \text{ [SA]} \end{aligned} \right\} \quad (15)$$

Substituting equation (14) into equation (12) (and setting  $\Gamma(2/3) = 1.354$ ) gives

$$\left. \begin{aligned} Nu_{loc,0} &= \frac{1.536(1 + 8.24\phi^{0.39})}{A^{1/3}(1 + 6.37\phi^{0.73})} Gz_{loc}^{1/3} = g Gz_{loc}^{1/3} \text{ [TA]} \\ Nu_{loc,0} &= \frac{1.224(1 + 4.40\phi^{0.39})}{A^{1/3}(1 + 2.66\phi^{0.73})} Gz_{loc}^{1/3} = g Gz_{loc}^{1/3} \text{ [SA]} \end{aligned} \right\} \quad (16)$$

Table 1. Asymptotic local Nusselt number in the region of small local Graetz number

$\sigma$	$Nu_{loc,\infty}$			
	Triangular array		Square array	
	This paper	Ref. [4]	This paper	Ref. [5]
1.001	—	1.42	—	—
1.01	2.14	2.11	1.51	—
1.02	2.78	2.74	1.74	—
1.05	4.92	4.91	2.31	—
1.1	8.75	8.80	3.11	—
1.2	11.62	11.74	4.32	—
1.25	—	—	—	5.50 <sup>a</sup>
1.5	7.49	7.58	4.74	5.10 <sup>a</sup>
2.0	4.41	4.47	3.45	3.44 <sup>a</sup>
4.0	2.04	—	1.67	—

<sup>a</sup> Values obtained by reading off Fig. 3 in ref. [5].

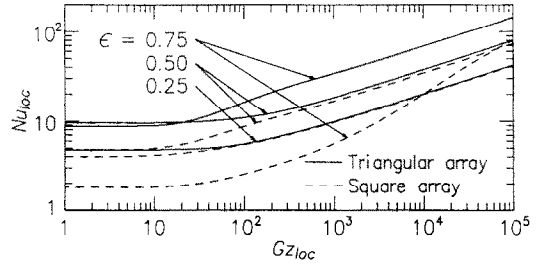


FIG. 7. Comparison of local Nusselt number between triangular and square arrays of cylinders.

As seen from Fig. 4, for  $\sigma < 1.1$  [TA] or 1.2 [SA],  $Nu_{loc}$  which shifts from  $Nu_{loc,0}$  to  $Nu_{loc,\infty}$  draws a logarithmic curve with an inflection point. Therefore, the interior division ratio  $\eta$  of  $Nu_{loc}$  between  $Nu_{loc,0}$  and  $Nu_{loc,\infty}$  is introduced, i.e.

$$\eta = \frac{Nu_{loc,0} - Nu_{loc}}{Nu_{loc} - Nu_{loc,\infty}}; Nu_{loc,0} \geq Nu_{loc} \geq Nu_{loc,\infty} \quad (17)$$

This equation may be rearranged in the form

$$\left. \begin{aligned} Nu_{loc} &= \frac{Nu_{loc,0} - Nu_{loc,\infty}}{1 + \eta} + Nu_{loc,\infty}; Nu_{loc,0} \geq Nu_{loc,\infty} \\ Nu_{loc} &= Nu_{loc,0}; Nu_{loc,0} < Nu_{loc,\infty} \end{aligned} \right\} \quad (18)$$

When  $\eta$  is expressed as simple as possible by using the least squares method, the following expressions are obtained:

$$\left. \begin{aligned} \eta &= 451 Gz_{loc}^{-(1.54\phi + 0.463)} = a Gz_{loc}^{\phi} \text{ [TA]} \\ \eta &= 94 Gz_{loc}^{-(7.66\phi + 0.281)} = a Gz_{loc}^{\phi} \text{ [SA]} \end{aligned} \right\} \quad (19)$$

Substituting equations (15), (16) and (19) into equation (18) gives

$$\left. \begin{aligned} Nu_{loc} &= \frac{g Gz_{loc}^{1/3} - f}{1 + a Gz_{loc}^{\phi}} + f; Gz_{loc} \geq \left( \frac{f}{g} \right)^3 \\ Nu_{loc} &= f; Gz_{loc} < \left( \frac{f}{g} \right)^3 \end{aligned} \right\} \quad (20)$$

Figure 8 shows a comparison between equation (20) (the solid curves) and the numerical solutions (the keyed symbols). The agreement is reasonably good showing that equation (20) is the satisfactory correlating equation for the

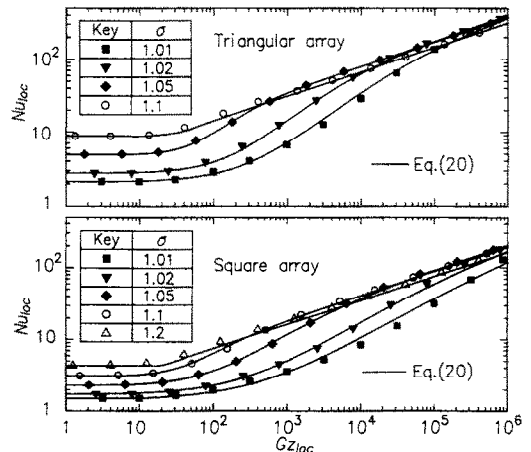


FIG. 8. Comparison of correlating equation (20) with numerical solutions for small pitch-to-diameter ratios.

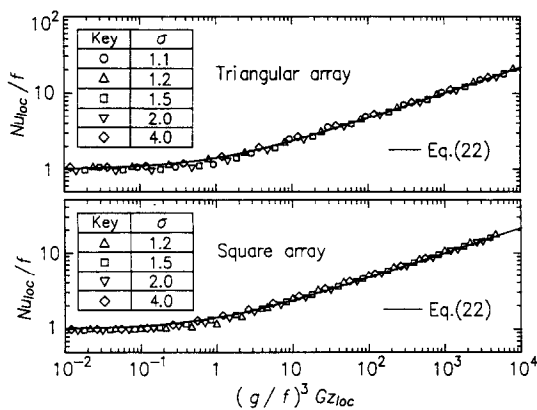


FIG. 9. Comparison of correlating equation (22) with numerical solutions for large pitch-to-diameter ratios.

local Nusselt number over the range  $\sigma = 1.01-1.1$  [TA] or  $\sigma = 1.01-1.2$  [SA].

On the other hand, for  $\sigma \geq 1.1$  [TA] or  $1.2$  [SA],  $Nu_{loc}$  shifts from  $Nu_{loc,0}$  to  $Nu_{loc,\infty}$  monotonously. Hence, the expression of the following form seems reasonable:

$$Nu_{loc} = (Nu_{loc,\infty}^2 + Nu_{loc,0}^2)^{1/2}. \tag{21}$$

Substituting equations (15) and (16) into equation (21) gives

$$Nu_{loc}/f = \{1 + (g/f)^2 Gz_{loc}^{2/3}\}^{1/2}. \tag{22}$$

Figure 9 indicates that equation (22), represented by the solid curves, is quite close to the numerical solutions represented by the keyed symbols, and is therefore a satisfactory correlating equation for the local Nusselt number over the range  $\sigma = 1.1-4.0$  [TA] or  $\sigma = 1.2-4.0$  [SA].

### 5. CONCLUDING REMARKS

A numerical analysis has been carried out to determine the characteristics of laminar-flow heat transfer to a fluid flowing axially between a triangular array [TA] or a square array [SA] of cylinders with a uniform wall heat flux and various pitch-to-diameter ratios  $\sigma$  (or dimensionless spacings  $\phi = \sigma - 1$ ). The relationship between the local Nusselt number  $Nu_{loc}$  and the local Graetz number  $Gz_{loc}$  was formulated, for  $\sigma = 1.01-1.1$  [TA] or  $\sigma = 1.01-1.2$  [SA] as

$$Nu_{loc} = \frac{g Gz_{loc}^{1/3} - f}{1 + 451 Gz_{loc}^{-(1.54\phi + 0.463)}} + f; \quad Gz_{loc} \geq \left(\frac{f}{g}\right)^3 \text{ [TA]}$$

$$Nu_{loc} = \frac{g Gz_{loc}^{1/3} - f}{1 + 94 Gz_{loc}^{-(7.66\phi + 0.281)}} + f; \quad Gz_{loc} \geq \left(\frac{f}{g}\right)^3 \text{ [SA]}$$

$$Nu_{loc} = f; \quad Gz_{loc} < (f/g)^3 \text{ [TA], [SA]},$$

and, for  $\sigma = 1.1-4.0$  [TA] or  $\sigma = 1.2-4.0$  [SA] as

$$Nu_{loc} = \{f^2 + g^2 Gz_{loc}^{2/3}\}^{1/2}$$

where

$$f = \frac{3.1\phi^{0.1} + 324\phi^{1.6}}{1 + 69.5\phi^{2.4}},$$

$$g = \frac{1.536(1 + 8.24\phi^{0.39})}{(2\sqrt{3\sigma^2 - \pi})^{1/3}(1 + 6.37\phi^{0.73})} \text{ [TA]}$$

$$f = \frac{3.6\phi^{0.2} + 32.2\phi^{1.5}}{1 + 9.1\phi^{2.2}},$$

$$g = \frac{1.224(1 + 4.40\phi^{0.39})}{(4\sigma^2 - \pi)^{1/3}(1 + 2.66\phi^{0.73})} \text{ [SA]}.$$

### REFERENCES

1. E. M. Sparrow, A. L. Loeffler, Jr. and H. A. Hubbard, Heat transfer to longitudinal laminar flow between cylinders, *J. Heat Transfer* **83**, 415 (1961).
2. C.-J. Hsu, Laminar- and slug-flow heat transfer characteristics of fuel rods adjacent to fuel subassembly walls, *Nucl. Sci. Engng* **49**, 398 (1972).
3. V. M. Borishanskii, M. A. Gotovskii and E. V. Firsova, Heat exchange when a liquid metal flows longitudinally through a bundle of rods arranged in a triangular lattice, *Atom. Energiya* **22**, 818 (1967).
4. O. E. Dwyer and H. C. Berry, Laminar-flow heat transfer for in-line flow through un baffled rod bundles, *Nucl. Sci. Engng* **42**, 81 (1970).
5. K. A. Antonopoulos, Heat transfer in tube assemblies under conditions of laminar axial, transverse and inclined flow, *Int. J. Heat Fluid Flow* **6**, 193 (1985).
6. O. Miyatake and H. Iwashita, Laminar-flow heat transfer to a fluid flowing axially between cylinders with a uniform surface temperature, *Int. J. Heat Mass Transfer* **33**, 417 (1990).
7. E. M. Sparrow and A. L. Loeffler, Jr., Longitudinal laminar flow between cylinders arranged in regular array, *A.I.Ch.E. Jl* **5**, 325 (1959).
8. R. B. Bird, Zur Theorie des Warmeebergangs an Nicht-Newtonsche Flussigkeiten bei Laminarer Rohrstromung, *Chemie-Ing.-Tech.* **31**, 569 (1959).
9. O. Miyatake and H. Iwashita, A numerical analysis of laminar-flow heat transfer in the thermal entrance region between cylinders with a uniform surface heat flux, *Rep. Res. Inst. Ind. Sci., Kyushu Univ.* No. 82, 139 (1987).